Polarized-Neutron Study of the Magnetic Moment Density in Antiferromagnetic $CuSO_4$†

F. MENZINGER,* D. E. COX, B. C. FRAZER, AND H. UMEBAYASHI‡
Brookhaven National Laboratory, Upton, New York
(Received 13 January 1969)

A determination of the spatial distribution of magnetic moment density in the antiferromagnet $CuSO_4$ has been made by means of the polarized-neutron-beam technique. Data collected at 4.5°K for two zones showed very large deviations in a number of cases from a smooth form-factor curve. Fourier transforms of the data revealed regions of substantial magnetic moment density (~ 0.05–$0.1\mu_B$) localized mainly between the Cu^{2+} ions and the SO_4^{2-} groups. The observation of appreciable concentrations of density in positions removed from the Cu^{2+} sites suggests the presence of relatively strong superexchange interactions through the SO_4^{2-} groups, as indicated also by the relatively high Néel point of about 36°K. In order to permit accurate analysis of the polarized-beam data, the crystal-structure parameters of $CuSO_4$ at 77°K were refined by least-squares analysis, and the errors in the calculated nuclear-structure factors were evaluated.

I. INTRODUCTION

In recent years polarized neutrons have been successfully used in accurate determinations of unpaired electron distributions in a number of ferromagnetic metals and alloys.[1–7] Under certain conditions, as first demonstrated in a striking study of covalent or delocalized spin density in MnF_2,[8,9] the polarized-beam technique is also applicable to antiferromagnets. The existence of such unpaired charge as detected in MnF_2 is related to the fundamental phenomenon of superexchange in insulating materials. The present paper describes the results of a detailed study of antiferromagnetic $CuSO_4$, which might be expected to show considerably more covalent character than a simple fluoride.

$CuSO_4$ is orthorhombic and undergoes an antiferromagnetic transition at about 35°K.[10–15] A recent powder neutron-diffraction study[16] revealed a magnetic structure consisting of antiferromagnetic chains along the c axis coupled parallel to neighboring moments in the (001) planes (Fig. 1), with the spin direction along the a axis. The Cu ions are in distorted octahedral sites, with the oxygen octahedra sharing edges to form the c-axis chains. The separation between Cu ions within a chain is 3.35 Å, but between chains is considerably greater ($\sim$4.8 Å). For long-range three-dimensional order to be established, exchange interactions via at least two oxygens are required. Uryu[17] has proposed an explanation of the magnetic structure on the basis of isotropic exchange and dipole interactions, but without considering interactions between corner and body-centered moments.

Like MnF_2, $CuSO_4$ is a favorable case for a polarized-beam study. The magnetic unit cell is the same size as the primitive chemical cell, and both nuclear- and mag-

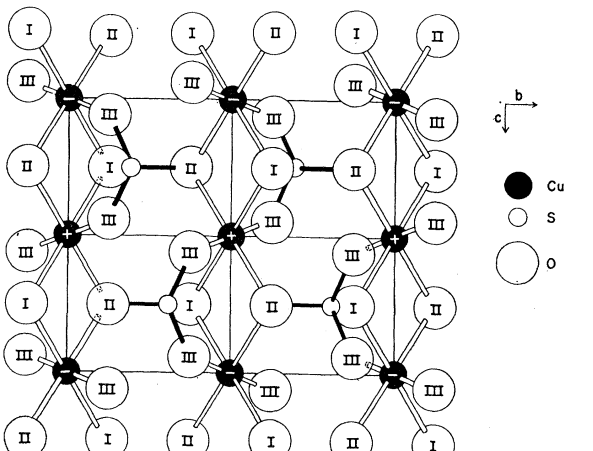

FIG. 1. Projection of the crystal structure of $CuSO_4$ onto (100). Short, broken line extensions to the bonds from Cu to O indicate that the oxygens in question lie directly beneath the ones actually shown. + and − signs signify Cu magnetic moments in the antiferromagnetic state.

† Work performed under the auspices of the U.S. Atomic Energy Commission.
* Permanent address: CSN Casaccia CNEN Rome, Italy.
‡ Permanent address: Central Laboratory, Tohoku Metal Company, Yokohama, Japan.

[1] S. J. Pickart and R. Nathans, Phys. Rev. **123**, 1163 (1961).
[2] C. G. Shull and Y. Yamada, J. Phys. Soc. Japan **17**, Suppl. B-III, 1 (1962).
[3] G. Shirane, R. Nathans, and C. W. Chen, Phys. Rev. **134**, A1547 (1964).
[4] R. M. Moon, Phys. Rev. **136**, A195 (1964).
[5] H. A. Mook, Phys. Rev. **148**, 495 (1966).
[6] C. G. Shull and H. A. Mook, Phys. Rev. Letters **16**, 184 (1966).
[7] F. Menzinger and A. Paoletti, Phys. Rev. **143**, 365 (1966).
[8] H. A. Alperin, P. J. Brown, R. Nathans, and S. J. Pickart, Phys. Rev. Letters **8**, 237 (1961).
[9] R. Nathans, H. A. Alperin, S. J. Pickart, and P. J. Brown, J. Appl. Phys. **34**, 1182 (1963).
[10] W. J. de Haas and C. J. Gorter, Commun. Kamerlingh Onnes Lab. Univ. Leiden **19**, 215a (1931).
[11] J. W. Stout, J. Chem. Phys. **9**, 285 (1941).
[12] A. S. Borovik-Romanov and N. M. Kreines, Zh. Eksperim. i Teor. Fiz. **33**, 1119 (1957) [English transl.: Soviet Phys.—JETP **6**, 862 (1958)].
[13] N. M. Kreines, Zh. Eksperim. i Teor. Fiz. **35**, 1391 (1958) [English transl.: Soviet Phys.—JETP **8**, 972 (1959)].
[14] T. Watanabe, J. Phys. Soc. Japan **16**, 1131 (1961).
[15] J. S. Wells, L. M. Matarrese, and D. J. Sukle, J. Chem. Phys. **47**, 2259 (1967).
[16] I. Almodovar, B. C. Frazer, J. J. Hurst, D. E. Cox, and P. J. Brown, Phys. Rev. **138**, A153 (1965).
[17] N. Uryu, J. Chem. Phys. **46**, 4868 (1967).

TABLE I. Least-squares refinement of atomic positions in $CuSO_4$ from 77°K neutron data. Standard deviations are given in parentheses. Scattering amplitudes taken as 0.79, 0.31, and 0.577×10^{-12} cm (Ref. 24).

	$x(\sigma_x)$	$y(\sigma_y)$	$z(\sigma_z)$	$B(\sigma_B)$ (Å^2)
Cu	0	0	0	0.21(7)
S	0.4565(21)	0.1847(13)	0.25	0.51(15)
O(I)	0.7375(12)	0.1315(6)	0.25	0.24(8)
O(II)	0.4362(11)	0.3679(5)	0.25	0.33(10)
O(III)	0.3095(13)	0.1297(4)	0.0650(4)	0.24(8)

netic-structure factors of appropriate phase contribute to each reflection (except for certain systematic glide-plane absences). However, an important difference is the much smaller Cu^{2+} moment, as compared with that of Mn^{2+}. With the latter, the regions of covalent spin density, corresponding to less than $0.1\mu_B$, are revealed only by the presence of "forbidden" magnetic reflections. Any contributions of this sort to the principal peaks are swamped by the much larger scattering from the localized moment of almost $5\mu_B$ on the Mn^{2+} ion. Analysis must therefore be based on a partial Fourier projection which utilizes only the forbidden reflections. As the present paper will show, covalency effects are detectable in both types of peaks in $CuSO_4$, in which the moment localized on the Cu^{2+} ion is only about $1\mu_B$.

II. EXPERIMENTAL DETAILS

A. Crystal Structure Refinement

The crystal selected for study was grown from solution in H_2SO_4 and $(NH_4)_2SO_4$ by Gruzensky, in the NBS Laboratories at Boulder, Colo.[18] Its dimensions were roughly $2\times3\times4$ mm^3. A crystal from the same batch was found to have lattice constants $\alpha=4.828$ Å, $b=8.397$ Å, $c=6.699$ Å, in good agreement with published data.[19,20] Since the polarized-beam technique requires an accurate knowledge of the nuclear-structure factors, data were collected at 77°K for a least-squares refinement of the crystal structure.

The space group for $CuSO_4$ is $Pbnm(D_{2h}^{16})$, with the atoms in the following positions: Cu in 4(a) at (0,0,0), S in 4(c) at $(x_1,y_1,\frac{1}{4})$, O(I) in 4(c) at $(x_2,y_2,\frac{1}{4})$, O(II) in 4(c) at $(x_3,y_3,\frac{1}{4})$, O(III) in 8(d) at (x_4,y_4,z_4).

The general reflection conditions for this space group are ($0kl$): k even, and ($h0l$): $h+l$ even. Ninety independent reflections were measured in the ($0kl$) and (hhl) zones. In the structure refinement, the data were weighted by the function $\sqrt{w}=1/(\sigma+0.05F_0)$, where σ is the standard deviation in the counting statistics and F_0 is the observed structure factor. Each F_0 was derived from observations of at least two and often four equivalent reflections, the intensities of which in most cases agreed to within 5–10%. Corrections for half-wavelength contamination were made where necessary. Eleven of the peaks were excluded from the final refinement because of extinction effects or because substantial uncertainty was introduced by overlap with aluminum peaks from the sample holder. Initial parameters were those obtained in the previous study.[16] The refined values, along with individual isotropic temperature parameters, are listed in Table I. Observed and calculated structure factors are listed in Table II. The weighted R factor $[\sum w(F_0-F_c)^2/\sum wF_0^2]^{1/2}$ is

TABLE II. Comparison of observed (F_0) and calculated (F_c) structure factors for $CuSO_4$ together with estimated standard deviations of the latter $\sigma(F_c)$ at 77°K. Parameters as in Table I. Peaks marked with an asterisk were excluded from refinement, as noted in text.

hkl	F_0	F_c	$\sigma(F_c)$	(hkl)	F_0	F_c	$\sigma(F_c)$
002	0.54	0.47	0.02	110	2.81	2.90	0.07
004*	6.57	8.50	0.13	111	3.11	3.23	0.07
006	5.47	−5.84	0.12	112	1.54	1.57	0.04
008	3.98	3.94	0.13	113	1.59	−1.65	0.04
				114	3.95	3.98	0.07
020	1.57	1.65	0.05	115	3.67	3.62	0.06
021	2.83	−2.73	0.05	116	3.09	3.03	0.06
022	4.45	4.17	0.08	117	2.43	−2.20	0.05
023	3.65	−3.38	0.07	118	4.53	4.68	0.08
024*	2.27	1.93	0.04	119	1.93	1.80	0.07
025	4.70	−4.82	0.09				
026	4.38	4.35	0.08	220	2.91	2.67	0.06
027	0.15	−0.36	0.07	221	4.42	4.43	0.09
				222	3.86	3.90	0.07
040	5.59	−5.96	0.11	223	0.35	0.20	0.05
041	1.27	1.38	0.05	224	2.44	2.42	0.05
042	4.52	4.56	0.09	225	5.29	5.95	0.11
043*	1.08	−0.64	0.06	226	3.40	3.44	0.06
044	1.23	−1.10	0.06	227	2.40	−1.98	0.10
045	1.62	1.55	0.05	228	2.03	2.17	0.07
046*	9.15	10.62	0.17	229	1.17	1.17	0.08
047	0.82	−0.88	0.05				
048	3.00	2.90	0.11	330*	0.82	−0.20	0.07
				331	1.12	−1.09	0.05
060	6.10	5.89	0.13	332	1.40	1.33	0.07
061*	1.35	1.06	0.06	333	2.39	−2.22	0.08
062	1.59	1.58	0.08	334	2.90	2.90	0.07
063	4.69	4.76	0.10	335	2.28	−2.25	0.07
064	5.08	4.93	0.10	336	5.43	5.45	0.10
065	3.16	3.18	0.09	337	0.58	−0.56	0.05
066*	0.60	0.49	0.07	338	6.24	5.25	0.13
067	1.74	1.70	0.09				
				440*	0.94	0.28	0.13
080*	8.53	10.25	0.16	441	0.88	0.89	0.04
081	0.46	−0.51	0.07	442	5.02	4.52	0.14
082	2.88	2.92	0.09	443	0.68	−0.76	0.05
083*	1.84	−0.85	0.12	444	1.04	1.03	0.06
084	5.31	5.62	0.12	445	0.83	0.88	0.04
085	1.18	−0.98	0.07	446	4.72	5.33	0.15
				447	0.97	−0.74	0.04
0,10,0	0.76	0.58	0.10				
0,10,1	0.92	−0.86	0.08	550	5.32	6.13	0.13
0,10,2	3.21	3.22	0.14	551	1.43	−1.37	0.08
0,10,3	4.31	−4.50	0.14	552	3.54	3.89	0.10
0,10,4	1.68	1.84	0.08	553	3.34	−3.06	0.13
				554	3.40	3.43	0.10
002	0.36	0.47	0.02	555	2.90	−2.92	0.11
004*	6.57	8.50	0.14				
006	5.43	−5.84	0.12	660	2.21	2.33	0.11
008	3.94	3.94	0.11	661	0.45	0.49	0.09
00,10	4.07	−4.42	0.17				

[18] P. M. Gruzensky, J. Res. Natl. Bur. Std. (U. S.) **68A**, 313 (1964).

[19] P. A. Kokkoros and P. J. Rentzeperis, Acta Cryst. **11**, 361 (1958).

[20] There is, however, a considerable discrepancy between the values of 6.699 and 6.69 Å obtained for c in the present work and in Ref. 18, respectively, and the value of 6.811 Å obtained by Pistorius, Am. Mineralogist **45**, 744 (1960).

TABLE III. Interatomic distances and angles in $CuSO_4$. Parameters as in Table I. N is the number of equivalent neighbors.

	Distance (Å)	N
Cu-O(I)	2.37	2
Cu-O(II)	2.03	2
Cu-O(III)	1.89	2
S-O(I)	1.43	1
S-O(II)	1.54	1
S-O(III)	1.51	2
	Bond angle (deg)	
O(I)-Cu-O(II)	75.7	
O(I)-Cu-O(III)	89.2	
O(II)-Cu-O(III)	89.6	
O(I)-S-O(II)	111.9	
O(I)-S-O(III)	111.2	
O(II)-S-O(III)	106.0	
O(III)-S-O(III)	110.4	

0.072. The estimate of the standard deviation of an observation of unit weight $[\sum w(F_0-F_c)^2/(n-m)]^{1/2}$, where n and m are, respectively, the number of observations and the variable parameters, has a value of 1.25, as compared with an ideal value of unity for properly chosen weights. This indicates that the errors estimated are realistic.

The values in Table I are generally in good agreement with those derived previously[16] from the Kokkoros and Rentzeperis room-temperature x-ray data,[19] although the x parameters of S and O(I) are shifted appreciably. Interatomic distances and bond angles are listed in Table III. One notable feature is the large distortion of the oxygen octahedra surrounding the Cu ions, with two long Cu-O distances of 2.37 Å and four shorter distances ranging from 1.89 to 2.03 Å. This can be attributed mainly to the large Jahn-Teller effect for a $3d^9$ ion in octahedral surroundings. The long axis of the octahedron is tilted roughly 15° from the normal to the plane containing the shorter axes. The SO_4 tetrahedra are less distorted, with S-O distances ranging from 1.43–1.54 Å and angles from 106°–112°.

B. Magnetic Symmetry and Structural Aspects

The basic magnetic structure determined in the powder study[16] consists of a collinear antiferromagnetic mode designated A_x,[21] with moments $S_1(+)$ at (0,0,0), $S_2(-)$ at $(0,0,\frac{1}{2})$, $S_3(+)$ at $(\frac{1}{2},\frac{1}{2},0)$, and $S_4(-)$ at $(\frac{1}{2},\frac{1}{2},\frac{1}{2})$. The magnetic reflection conditions are $h+k$ even and l odd. Hence reflections in the two zones studied, $(0kl)$ and (hhl), would be expected to fall into three categories: purely magnetic peaks $(00l)$ with l odd; peaks with both nuclear and magnetic contributions, such as $(0kl)$ with k even and l odd which are polarization sensitive; and purely nuclear (or magnetically "forbidden") peaks, such as $(0kl)$ with both k and l even. However, the absence in general of magnetic contributions to peaks in the latter category is conditional upon the magnetization density being spherical and localized upon the Cu^{2+} ion. The data to be described in Sec. III show clearly in fact that this condition is violated and the simple model above is inadequate.

There is a more generalized model with Pbnm symmetry in which some fraction of the magnetization density distribution is represented by moments placed in general $8(d)$ positions. The operation of the appropriate magnetic symmetry elements[22] yields an antiferromagnetic mode A_x' with the structure factor expression

$$F_M(hkl) \propto \sin 2\pi[\tfrac{1}{4}(h+k+l)-ky] \times \sin 2\pi(\tfrac{1}{4}l-lz)\cos 2\pi[\tfrac{1}{4}(h+k)-hx].$$

The reflection conditions are now $(0kl)$ $k=2n$, $l\neq 0$; (hhl) $l\neq 0$; and $(00l)$ $l=2n+1$. In addition, the signs of F_M for equivalent reflections, which are determined directly once the signs of the nuclear-structure factors are known, are as follows:

$$F(hkl)=F(\bar{h}kl)=F(h\bar{k}l)=F(hk\bar{l})=F(\bar{h}\bar{k}\bar{l}),\ l \text{ odd}$$
$$F(hkl)=F(\bar{h}kl)=-F(h\bar{k}l)=-F(hk\bar{l})=F(\bar{h}\bar{k}\bar{l}),\ l \text{ even}.$$

From magnetic-symmetry[22] or group-theoretical[21] arguments it can also be shown that there is the possibility of additional antiferromagnetic modes G_y and C_z being coupled with the basic A_x mode. Anisotropic forces could produce coupling of this sort and, although the components would not be expected to be large, a canted arrangement has been detected in $CuCl_2\cdot 2D_2O$,[23] for example, with a minor component of roughly $0.1\mu_B$. However, for both G and C modes, one of the reflection conditions is that $h+k$ should be odd, and polarized-beam data taken in the $(0kl)$ and (hhl) zones would therefore not be affected in either case.

There is, though, a possible complication in the generalized case from the modes G' and C' analogous to A'. Although the $(0kl)$ data would still not be affected, the possibility of some interference with the (hhl) reflections cannot altogether be ruled out, and will be considered later.

C. Magnetic Data

Most of the magnetic intensities were measured by the polarized-beam technique, but a few peaks in the $(0kl)$ zone were also measured, both at liquid-nitrogen and liquid-helium temperatures with unpolarized neutrons. The resulting magnetic structure factors $|F_M|$ obtained by subtraction of the liquid-nitrogen from the liquid-helium data confirmed the previously reported magnetic structure.[16] These F_M values were also used to determine the domain distribution in the polarized-beam experiment for the $(0kl)$ zone. However,

[21] E. F. Bertaut, in *Magnetism*, edited by G. T. Rado and H. Suhl (Academic Press Inc., New York, 1963), Vol. III. Note that S_3 and S_4 have been interchanged in the present paper.

[22] G. Donnay, L. M. Corliss, J. D. H. Donnay, N. Elliott, and J. M. Hastings, Phys. Rev. **112**, 1917 (1968).

[23] H. Umebayashi, B. C. Frazer, D. E. Cox, and G. Shirane, Phys. Rev. **167**, 519 (1968).

TABLE IV. Neutron data for the (0*kl*) zone of $CuSO_4$ at 4.5°K. Except where overlap with other peaks is suspected, errors in γ given are standard deviations of counting statistics. F_N, F_M(obs), and F_M(calc) are in units of 10^{-12} cm per unit cell. F_M(calc) includes both spherical and aspherical terms, as described in text. Errors in F_M(obs) include allowance for those in F_N, as listed in Table II. Magnetic, nuclear-magnetic, and "forbidden" reflections designated m, nm, and f, respectively.

0*kl*	$(\sin\theta)/\lambda$ (Å^{-1})	γ	F_N	F_M(obs)	F_M(calc)	Type
001	0.075	...	...	0.995±0.007	1.04	m
020	0.119	0.000 ±0.001	1.650	0.000±0.002	...	f
021	0.140	−0.280 ±0.017	−2.726	0.763±0.049	0.92	nm
002	0.149	0.000 ±0.004	0.474	0.000±0.002	...	f
022	0.191	−0.0003±0.0008	4.171	−0.001±0.003	0.06	f
003	0.224	...	...	0.690±0.030	0.82	m
040	0.238	−0.003 ±0.002	−5.960	0.018±0.013	...	f
041	0.250	0.528 ±0.004	1.375	0.726±0.027	0.66	nm
023	0.254	−0.169 ±0.011	−3.378	0.571±0.039	0.74	nm
042	0.281	0.013 ±0.002	4.563	0.060±0.009	0.10	f
004	0.299	−0.001 ±0.002	8.499	−0.01 ±0.02	...	f
024	0.322	−0.004 ±0.004	1.926	−0.008±0.008	0.04	f
043	0.327	0.108 ±0.009	0.641	0.069±0.009	0.56	nm
060	0.358	0.001 ±0.003	5.892	0.006±0.015	...	f
061	0.365	0.386 ±0.007	1.059	0.409±0.024	0.39	nm
005	0.374	...	...	0.50 ±0.08	0.59	m
062	0.388	0.030 ±0.006	1.585	0.048±0.010	0.12	f
025	0.392	−0.063 ±0.002	−4.823	0.304±0.011	0.54	nm
063	0.422	0.079 ±0.004	4.764	0.376±0.021	0.33	nm
045	0.443	0.217 ±0.002	1.549	0.336±0.011	0.43	nm
006	0.448	0.001 ±0.003	−5.841	−0.006±0.016	...	f
026	0.464	0.006 ±0.003	4.348	0.026±0.015	0.00	f
064	0.466	0.014 ±0.003	4.933	0.069±0.015	0.12	f
081	0.483	−0.324 ±0.024	−0.506	0.164±0.026	0.16	nm
082	0.500	0.018 ±0.004	2.923	0.053±0.012	0.12	f
046	0.508	0.004 ±0.003	10.624	0.042±0.031	0.01	f
065	0.516	0.093 ±0.002	3.175	0.295±0.010	0.30	nm
007	0.523	...	...	0.24 ±0.12	0.44	m
083	0.527	−0.118 ±0.021	0.845	0.100±0.023	0.16	nm
027	0.537	−0.258 ±0.033	−0.356	0.092±0.021	0.41	nm
084	0.563	0.009 ±0.003	5.625	0.051±0.020	0.15	f
047	0.575	−0.37 ±0.06	−0.882	0.326±0.056	0.35	nm
0,10,1	0.601	−0.129 ±0.015	−0.857	0.111±0.017	0.02	nm
085	0.606	−0.207 ±0.011	−0.978	0.202±0.018	0.16	nm
067	0.634	0.127 ±0.004	1.699	0.216±0.013	0.26	nm
0,10,3	0.637	−0.026 ±0.003	−4.501	0.117±0.014	0.03	nm
048	0.644	−0.004 ±0.003	2.901	−0.016±0.009	−0.05	f
029	0.683	0.064 ±0.007	1.309	0.084±0.018	0.34	nm
0,10,5	0.703	−0.051 ±0.003	−2.813	0.143±0.009	0.06	nm
049	0.714	0.027 ±0.030	0.691	0.019±0.022	0.27	nm

this procedure was not possible for the (*hhl*) zone owing to the less favorable orientation of the spin axis and the, consequently, lower accuracy of the unpolarized neutron measurements.

The quantity measured directly in a polarized neutron experiment is the polarization ratio R_P, which is the ratio of the intensities measured with the neutron polarization vector, respectively, parallel and antiparallel to the magnetic guide field.[9] For an antiferromagnet,

$$R_P=\frac{F_N^2+F_M^2q^2+2APF_NF_M\mathbf{q}\cdot\boldsymbol{\lambda}}{F_N^2+F_M^2q^2-2AP\varphi F_NF_M\mathbf{q}\cdot\boldsymbol{\lambda}}=\frac{1+\gamma^2q^2+2AP\gamma\mathbf{q}\cdot\boldsymbol{\lambda}}{1+\gamma^2q^2-2AP\varphi\gamma\mathbf{q}\cdot\boldsymbol{\lambda}},\quad(1)$$

where F_N and F_M are the nuclear and magnetic structure factors, respectively, $\gamma=F_M/F_N$, A is the difference between the fractional volumes occupied by the two possible domain types, P is the degree of polarization of the incident beam, φ is the efficiency of the polarization reversal process, and $\mathbf{q}$ and $\boldsymbol{\lambda}$ have their usual significance (Bacon).[24]

Polarized neutron data were collected at 4.5°K for two zones, (0*kl*) and (*hhl*). In the (0*kl*) case, the difference in domain population A (or strictly speaking, the product AP, since P is not known precisely) was obtained in two ways: by direct comparison with the unpolarized neutron data and by temperature dependence measurements. In the latter case, F_M for a purely magnetic peak such as (001) and R_P for a number of polarization-sensitive reflections were measured as functions of temperature. The reduced (γ,T) curves were then fitted to the (F_M,T) curve by treating AP as a variable parameter and assuming the same temperature dependence for all reflections. The two methods gave consistent results for the domain population. The population varied somewhat on cycling through the Néel temperature, but a typical value found for AP was

[24] G. E. Bacon, *Neutron Diffraction* (Clarendon Press, Oxford, England, 1962).

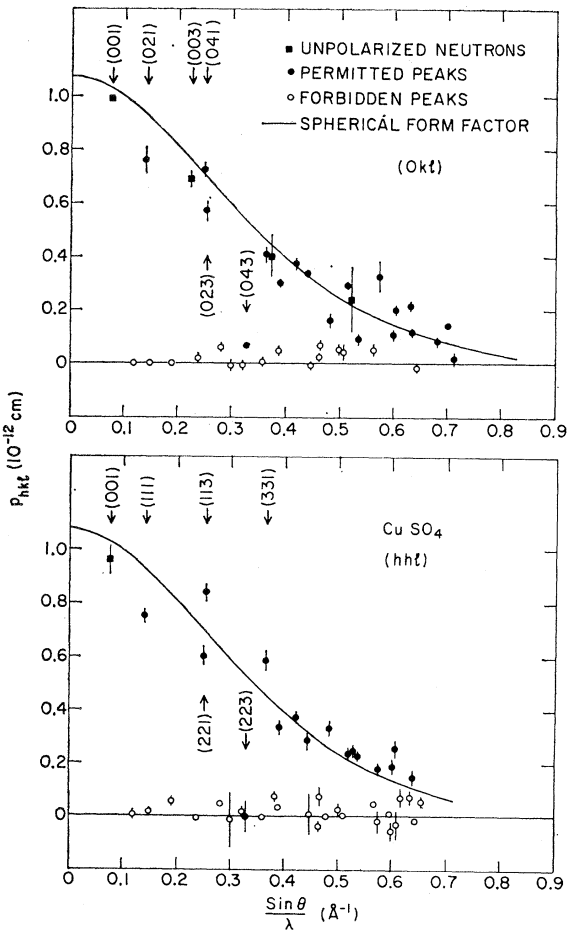

FIG. 2. Form factors for the (0*kl*) and (*hhl*) zones of $CuSO_4$. The smooth curve represents the theoretical spherical form factor for Cu^{2+}: R. E. Watson (private communication).

0.78±0.02. The Néel temperature was found to be 36.3±1.0°K.

Data for the (0*kl*) zone are given in Table IV and in the form-factor plot in Fig. 2. The estimated errors in the data are discussed critically in Sec. II D.

The presence of small magnetic contributions to the magnetically forbidden peaks (*k* and *l* both even) show at once that the simple localized spherical model is not valid. However, the most significant feature of Fig. 2 is not the presence of the forbidden peaks but the fact that a number of the observed F_M values of the low-angle nuclear-magnetic reflections deviate widely from any smooth form-factor curve one might attempt to fit to the data. For comparison purposes, a spherical Cu^{2+} form factor is drawn into the figure. There are particularly noticeable deviations for (021), (023), and (043). Moreover, these peaks occur at values of $(\sin\theta)/\lambda$, too low for the deviations to be accounted for by inclusion of aspherical terms in the Cu^{2+} form factor, and are indicative of some unpaired charge distribution in general positions of the unit cell.

In order to collect data in the (*hhl*) zone it, was necessary to heat the sample to room temperature for remounting. A direct determination of the new domain population could not be made with sufficient accuracy to properly scale the magnetic-structure factors, either by comparison with the unpolarized data or by temperature-dependence measurements. For the (*hhl*) setting, the spin axis is tilted by about 60° from the zone axis; hence the magnetic contributions average only 25% of those observed in the (0*kl*) zone, which were already quite weak. The following approach was therefore used. A value of AP within the error limits of the direct determination was chosen so as to roughly minimize the deviations from a spherical form factor. This procedure gave a value of 0.45±0.05 and the corresponding results are shown in Table V and Fig. 2. Variation of AP over a quite wide range does not radically change the picture.

Once again, there are large deviations from a spherical Cu^{2+} form factor, much greater than many of the error bars. Thus, in agreement with results for the other zone, there is a clear indication of appreciable accumulations of magnetization density removed from the Cu^{2+} sites in the unit cell.

An examination of the data in Tables IV and V reveals that except in one or two marginal cases, peaks not satisfying the generalized reflection conditions for the A' mode mentioned previously are within error limits systematically zero. Furthermore, a check on a number of reflections showed that in all cases the signs of the structure factors of equivalent reflections were also in accordance with the assumption of a generalized collinear spin distribution of *Pbnm* symmetry.

D. Consideration of Systematic Errors

Since some of the observed form-factor values show deviations much larger than any reported before, careful consideration was given to possible sources of systematic experimental errors as follows.

1. Errors in Nuclear-Structure Factors

Since the determination of F_M from γ requires a knowledge of F_N, the accuracy with which the latter is known comes into question. Most investigations to date have dealt with simple ferromagnetic metals or alloys for which the crystal structures were known exactly. Thus, no errors were introduced by the use of calculated values of F_N other than those which could result from an imprecise knowledge of scattering lengths. The nature of the problem is rather different for antiferromagnetic compounds such as $CuSO_4$, however, where in order for a polarization effect to be produced at all, crystal structures of some complexity must be involved. In such a case, the reliability of the structure determination must be considered, and a quantitative estimate of the standard deviations in the calculated values of F_N made. There is a straightforward means for doing this, since the required errors are in fact

TABLE V. Neutron data for the (*hhl*) zone. Notation as in Table IV.

hhl	$(\sin\theta)/\lambda$ (Å^{-1})	γ	F_N	F_M(obs)	F_M(calc)	Type
001	0.075	...	...	0.964±0.050	1.04	m
110	0.119	0.002 ±0.005	2.897	0.006±0.014	...	f
111	0.141	0.233 ±0.006	3.231	0.753±0.025	0.93	nm
002	0.149	0.039 ±0.016	0.474	0.018±0.008	...	f
112	0.191	0.034 ±0.011	1.569	0.058±0.011	0.03	f
220	0.239	−0.002 ±0.006	2.667	−0.005±0.006	...	f
221	0.250	0.136 ±0.005	4.429	0.602±0.025	0.69	nm
113	0.254	−0.508 ±0.018	−1.654	0.840±0.036	0.74	nm
222	0.282	0.013 ±0.0015	3.899	0.051±0.006	0.06	f
004	0.299	−0.001 ±0.010	8.499	−0.01 ±0.10	...	f
114	0.322	0.005 ±0.004	3.976	0.020±0.015	0.02	f
223	0.327	−0.25 ±0.03	0.202	−0.050±0.014	0.54	nm
330	0.358	0.003 ±0.030	−0.202	−0.001±0.008	...	f
331	0.366	−0.535 ±0.021	−1.093	0.585±0.035	0.45	nm
224	0.383	0.032 ±0.004	2.424	0.077±0.010	0.06	f
332	0.388	0.028 ±0.004	1.330	0.037±0.006	0.08	f
115	0.392	0.093 ±0.007	3.623	0.337±0.026	0.52	nm
333	0.423	−0.169 ±0.010	−2.224	0.375±0.026	0.33	nm
225	0.444	0.048 ±0.006	5.950	0.286±0.036	0.39	nm
006	0.448	−0.002 ±0.014	−5.841	0.01 ±0.08	...	f
116	0.464	−0.012 ±0.005	3.027	−0.036±0.015	0.00	f
334	0.467	0.027 ±0.010	2.904	0.078±0.029	0.10	f
440	0.478	0.009 ±0.005	0.284	0.003±0.002	...	f
441	0.484	0.375 ±0.025	0.886	0.332±0.027	0.27	nm
442	0.501	0.006 ±0.005	4.518	0.027±0.022	0.10	f
226	0.508	0.007 ±0.001	3.436	0.024±0.004	0.02	f
335	0.518	−0.106 ±0.011	−2.246	0.238±0.026	0.23	nm
443	0.528	−0.330 ±0.029	−0.759	0.250±0.027	0.20	nm
117	0.537	−0.105 ±0.010	−2.197	0.231±0.023	0.40	nm
444	0.567	0.049 ±0.004	1.029	0.050±0.005	0.12	f
336	0.574	−0.003 ±0.007	5.452	−0.016±0.038	0.05	f
227	0.575	0.093 ±0.009	−1.976	0.184±0.020	0.29	nm
550	0.597	0.002 ±0.001	6.128	0.013±0.005	...	f
008	0.598	−0.013 ±0.008	3.936	−0.051±0.031	...	f
551	0.602	−0.138 ±0.018	−1.367	0.189±0.027	0.16	nm
445	0.607	0.291 ±0.035	0.880	0.256±0.033	0.18	nm
118	0.610	−0.006 ±0.011	4.678	−0.028±0.051	−0.02	f
552	0.616	0.019 ±0.009	3.893	0.074±0.035	0.10	f
337	0.634	−0.132 ±0.040	−0.560	0.074±0.023	0.17	nm
553	0.638	−0.049 ±0.010	−3.064	0.150±0.031	0.10	nm
228	0.644	0.0055±0.0027	2.171	−0.012±0.006	−0.01	f
446	0.655	0.0118±0.0022	5.333	0.059±0.012	0.09	f

given by the diagonal elements of the moment matrix in the least-squares refinement,

$$\hat{M}_F = A\hat{M}_x A'.$$

The notation is that used by Hamilton,[25] where A is the design matrix with elements $\{a_{ij}\} = \{\partial F_i/\partial x_j\}$, and $\hat{M}_x$ is the variance-covariance matrix of the least-squares parameters estimates. These quantities are available from storage in the least-squares program,[26,27] although as far as is known they have not been utilized before for this purpose. The program can be modified in a simple way to permit calculation of the errors in F_N, which are listed in Table II for the least-squares parameters of Table I. The magnitude of these errors is of the order of a few percent in most cases, which is comparable with the general level of statistical uncertainty in γ at lower angles, and even considerably more in a few cases.

[25] W. C. Hamilton, *Statistics in Physical Science: Estimation, Hypothesis Testing, and Least Squares* (Ronald Press Co., New York, 1964).

[26] W. R. Busing and H. A. Levy, Oak Ridge National Laboratory Report No. ORNL 59-4-37, 1959 (unpublished).

Since there are considerable differences in the scattering lengths quoted for Cu (0.79[28] and 0.746[29]$\times 10^{-12}$ cm) and S (0.31[30] and 0.28[31]$\times 10^{-12}$ cm), a further refinement was carried out in which these scattering lengths were also treated as variable parameters. This yielded values of 0.78±0.02 and 0.30±0.02$\times 10^{-12}$ cm, respectively, with the other parameters virtually unchanged. The corresponding errors in F_N differed very little from those in Table II. The latter have therefore been used in the calculation of the over-all errors in F_M listed in Tables IV and V.

2. *Depolarization Effects*

The degree of polarization of the beam at the sample position was not known accurately in the present

[27] J. A. Ibers and W. C. Hamilton, Acta Cryst. **17**, 781 (1964).

[28] D. T. Keating, W. J. Neidhardt, and A. N. Goland, Phys. Rev. **111**, 261 (1958).

[29] D. Bally, S. Todireanu, S. Ripeanu, and M. G. Belloni, Rev. Sci. Instr. **33**, 916 (1962).

[30] C. G. Shull and E. O. Wollan, *Solid State Physics* (Academic Press Inc., New York, 1956), Vol. 2, p. 143.

[31] N. Menyuk, K. Dwight, and A. Wold, J. Appl. Phys. **36**, 1088 (1965).

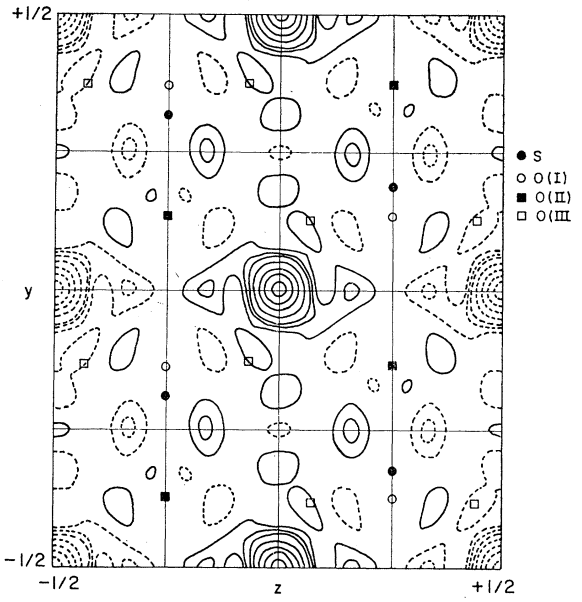

FIG. 3. Fourier projection of magnetization density on (100). Broken lines correspond to negative regions of magnetization. Contours are at following intervals: 50, 100, 150, 300, 500, 700, 900. The 100 level corresponds to a projected density of roughly $0.18\mu_B/\text{Å}^2$.

experiment. The usual technique of measuring the diffracted beam with an analyzing crystal gave only an approximate figure, since there was some depolarization between sample and analyzing crystal resulting from the absence of a guide field in the region occupied by the Dewar. A lower limit for P was about 90%. It is not necessary to know P independently, however, since what concerns us is the product of P and A, as it appears in formula (1) for the polarization ratio, and it is this factor which was determined experimentally as previously described.

3. Tilting of the Neutron Direction

In the absence of a guide field at the crystal, some deviation of the neutron spin axis from the vertical can also occur. Initially, the fringing fields of the magnetic collimator, which was placed as close as possible to the side of the Dewar, were relied upon to maintain the direction of polarization, and some deviation might be expected by the time the beam reaches the crystal. However, this uncertainty does not affect the $(0kl)$ results at all, since in this case the crystal spin axis is vertical and $\mathbf{q}\cdot\boldsymbol{\lambda}=-\mathbf{k}\cdot\boldsymbol{\lambda}$. Thus, any tilting of the neutron spin direction would act only to reduce its vertical component along $\mathbf{k}$, and the effect would be equivalent to a small decrease in the degree of polarization. The situation is different in the case of the (hhl) projection, however, for $\mathbf{k}$ is now about 60° from the vertical, and $\mathbf{q}\cdot\boldsymbol{\lambda}$ is not the same for different scattering directions. As a result reflections such as (hhl) and $(\bar{h}\bar{h}\bar{l})$ are no longer equivalent. An appreciable effect of this sort was in fact observed at first, and the fringe field at the crystal was modified by means of additional corrective magnets to minimize the differences between (hhl) and $(\bar{h}\bar{h}\bar{l})$ peaks. Data were corrected for the small effect still present.

4. Extinction

The results in Table II show that extinction effects are quite small generally, and negligible at the level of the magnetic intensities. Some of the more important polarization-sensitive reflections were also checked by making measurements at a wavelength of 0.85 Å but no discernible effects could be detected.

5. Multiple Scattering

It was not possible to investigate the effect of multiple scattering in any detail by rotation of the crystal around the scattering vector in the usual way because of the difficulty in tilting the Dewar through large angles. Moreover, in an antiferromagnetic crystal, the spin axis will also rotate and the magnetic-structure factor will depend upon the small horizontal component of the neutron polarization which, as described above, could not be eliminated or measured very accurately. However, a partial check was carried out for (021) and (041) by rotation of the crystal about ±5° around the scattering vector. No effect was found for (041), whereas (021) showed a variation in R_P of 6±2% of which at least part can be ascribed to tilting to the neutron spin axis. Since multiple scattering is also dependent upon the neutron wavelength, nine reflections were checked both at 1.05 and 0.95 Å, and four of these also at 0.85 Å (Table VI). Apart from a change of 4±2% in R_P for (023), none of the others showed changes outside statistical-error limits. Multiple scattering therefore does not appear to be a serious problem in this case.

6. Bragg Scattering from the Cryostat

The most troublesome aspect of this arises from the presence of suitably oriented large grains in the aluminum thermal radiation shielding and sample holder. Although the effect was minimized by the use of relatively large-diameter radiation shields, so that Bragg-

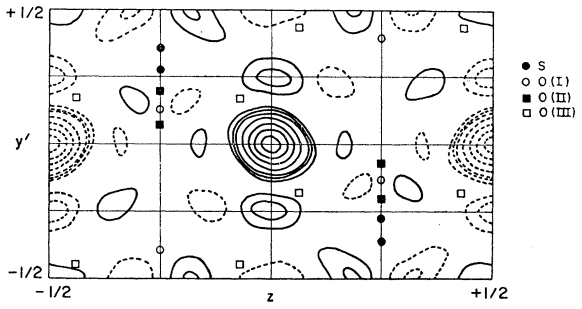

FIG. 4. Fourier projection of magnetization density on the plane normal to (001) and (110). Contours as in Fig. 3.

TABLE VI. Wavelength dependence of the polarization ratio (R_P).

hkl	F_N (10^{-12} cm)	R_P ($\lambda=1.05$ Å)	R_P ($\lambda=0.85$ Å)
021	−2.73	0.433±0.005	0.426±0.005
041	1.38	4.40 ±0.08	4.39 ±0.18
023	−3.38	0.606±0.007	0.582±0.007
043	−0.64	0.068±0.003	0.077±0.003

reflected neutrons from most of the aluminum could not reach the counter through the collimator, it could not be eliminated entirely. Therefore, in the region of the scattering angles where aluminum peaks would be expected, all equivalent reflections from the sample crystal were measured, and in addition, integrated reflection polarization ratios were measured and compared with the peak ratios. In a number of such cases the magnetic-structure factors have been assigned a larger error to allow for uncertainties of this sort.

III. DATA ANALYSIS AND DISCUSSION

The preceding experimental results have shown the presence of large deviations from a spherical form factor in $CuSO_4$. Analysis must take into account the possibility of both an aspherical magnetic moment density around the Cu^{2+} ion and the presence of appreciable densities in other regions of the unit cell. Both effects have been detected in previous neutron diffraction studies of antiferromagnetics, the former in NiO,[32] for example, and the latter in MnF_2.[9] However, the effects observed in the present study are far more pronounced, particularly since the "allowed" magnetic peaks at low angles are most affected.

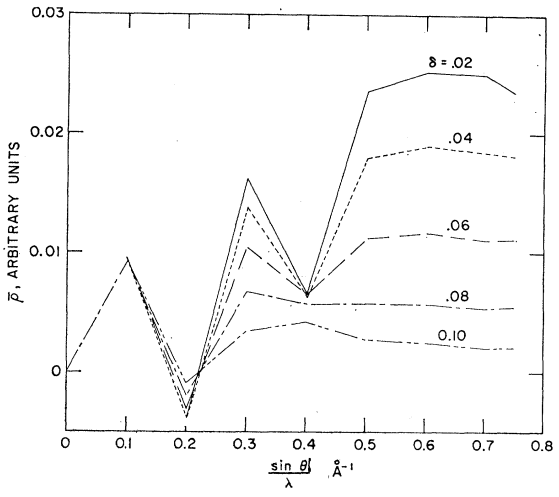

FIG. 5. Variation of $\bar{\rho}$, the projected magnetization density averaged over a rectangle of side 2δ centered at the point (0.25, 0.16), as a function of the number of reflections used in the Fourier synthesis. δ is expressed as a fraction of the projected cell edges.

[32] H. A. Alperin, J. Phys. Soc. Japan **17**, Suppl. B-III, 12 (1962).

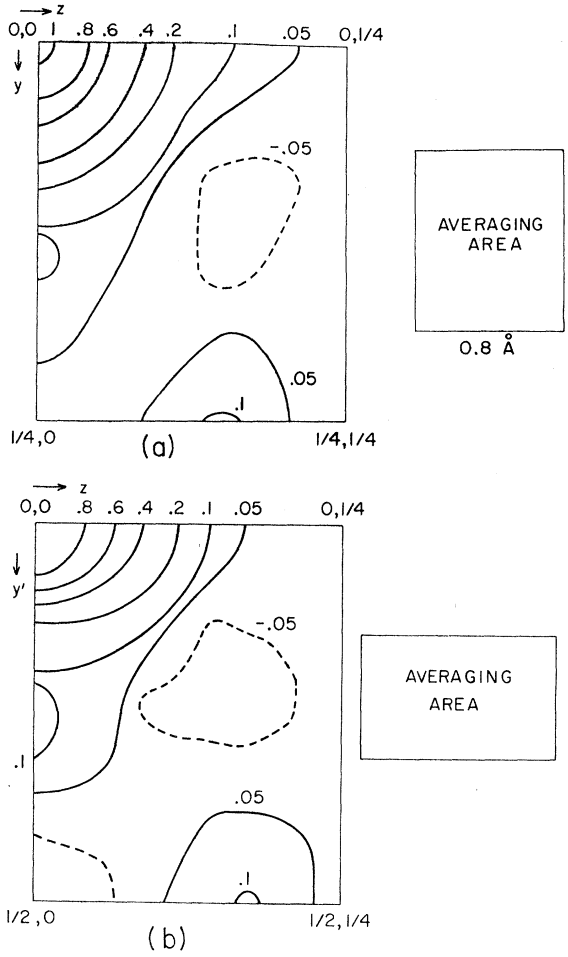

FIG. 6. Fourier projection of the averaged magnetization density $\bar{\rho}$ for (a) $(0kl)$ zone, (b) (hhl) zone. Contours are in units of $\mu_B/\text{Å}^2$.

The most direct analysis is yielded by a Fourier inversion of the structure factors, since these can be considered as coefficients in the Fourier expansion of the magnetic moment density (or the projected density in the case of a single zone). In the analysis of a polarized-beam experiment there is no phase problem since the sign of the magnetic-structure factor is measured relative to the known sign of the nuclear-structure factor.

The results of the inversion for the $(0kl)$ zone are shown in Fig. 3 as a projection of the magnetic moment density on the basal plane (100), and Fig. 4 shows the corresponding projection for the (hhl) zone. The axis of the latter projection is therefore at an angle

$$\theta=\cos^{-1}a/(a^2+b^2)^{1/2}=60.1°$$

from the a axis and orthogonal to the c axis. As can be seen in both projections there is a marked asphericity of the density in the immediate vicinity of the Cu ions together with regions of appreciable density at projected distances of about 2.5 Å from the Cu ions,

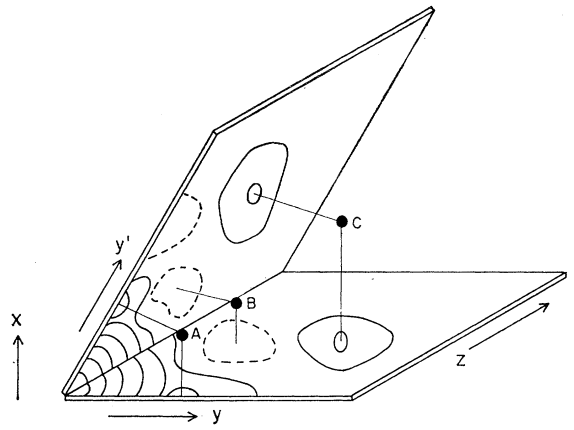

FIG. 7. Combined (0*kl*) and (*hhl*) projections showing correlation of extra regions of spin density, centered roughly at *A*, *B*, and *C*, which have the approximate coordinates 0.12, 0.14, 0; 0.10, 0.12, 0.16; and 0.25, 0.25, 0.16, respectively.

which clearly cannot be attributed to an extension of the Cu^{2+} unpaired 3*d* electron distribution.

A well-known drawback of the Fourier method is the presence of diffraction termination effects caused by the use of a finite amount of data. Recent work on the ferromagnetic 3*d* metals by Moon,[4] Mook,[5] and Shull and Mook[6] has shown that these effects can be greatly reduced by averaging the magnetic moment density over a small but finite volume. The resulting picture of the spatial density distribution is thus less detailed but more reliable than one obtains in a conventional Fourier synthesis. In the present case, data were collected out to $(\sin\theta)/\lambda$ values of 0.75 $Å^{-1}$ for the (0*kl*) zone and 0.65 $Å^{-1}$ for the (*hhl*) zone. The average projected density over an area of side 2δ (expressed as a fraction of the projected unit-cell lattice parameters) is given in the former case by

$$\bar{\rho}(y,z)=(1/A)\sum_k\sum_l F(0kl)\frac{\sin 2\pi k\delta}{2\pi k\delta}\times\frac{\sin 2\pi l\delta}{2\pi l\delta}\cos 2\pi(ky+lz),$$

where $A=bc$ and the $F(0kl)$'s are the observed magnetic-structure factors in Bohr magnetons. The convergence of this series for a given value of δ can be tested by variation of the number of reflections included in the summation. The results of this process for a typical point in the (0*kl*) plane are shown in Fig. 5, and a reasonable degree of convergence is obtained for $\delta=0.06$. For the (*hhl*) zone the expression must be modified slightly such that $A=abc/(a^2+b^2)^{1/2}$, k is replaced by h, and y is replaced by $x+y$. In this case, satisfactory convergence is reached at a value of 0.08 for δ due to the smaller limiting value of $(\sin\theta)/\lambda$.

The averaged projections are shown in Figs. 6(a) and 6(b), respectively. Some smearing of the detail in the averaged density maps is evident when compared to the point density maps (Figs. 4 and 5). Some of the minor peaks have disappeared and may therefore be considered insignificant. However, all of the main peaks are still present. This process was repeated after replacing the experimental values for (043) and (023), which show the largest deviations, by the theoretical spherical values. Most of the peak heights were affected by this change, as might be expected, but once again, all of the main peaks were still present.

The most significant feature of all is the existence of striking internal consistency between the two sets of independent data, as clearly revealed on the schematic diagram in Fig. 7. This is a composite of the two projections in Fig. 6. There is a close correlation in the sign, magnitude, and position of the extra peaks except for the upper negative region in the (*hhl*) projection. However, in this case, the corresponding region in the (0*kl*) projection may be lost in the contours around one of the Cu positions. This agreement shows also that neglect of the possible noncollinearities described earlier in the analysis of the (*hhl*) data has not introduced any serious discrepancies.

A comparison of observed and calculated aspherical form-factor values was also made. In the case of $CuCl_2\cdot 2D_2O$ [23] deviations from a spherical form factor can be accounted for to a large extent in this way. Although no such agreement in the present case was anticipated at least at low angles, the calculation was made in order to determine the general trends. The *z* axis of the Cu^{2+} ion was assumed to lie along the longest of the Cu-O bonds in the surrounding oxygen octahedron (see Table III), and the single 3*d* hole in the Cu^{2+} shell was assumed to occupy a pure E_g orbital of x^2-y^2 type. It is evident from Fig. 3 that these simple assumptions are reasonable, as the spin density is more compressed along the Cu-O(I) bond. Since the choice of orientation for the *x* and *y* axes was not at all clearcut (which is relevant because each of the four Cu^{2+} ions in the unit cell has a differently oriented environment), several alternatives were tried. Although a reasonable measure of agreement with the forbidden reflections alone can be obtained in this way, the over-all fit is poor for the orientations tried (Tables IV and V). This once again is indicative of a situation in which there are regions of substantial magnetic moment density localized sufficiently well to contribute to the high-angle reflections, but which are too far removed from the Cu^{2+} sites to be considered as part of the asphericity. The fact that there is better agreement for the forbidden reflections appears to be more of a coincidence resulting from the particular positions occupied by the extra density.

An accurate determination of the magnetization present in the extra peaks cannot be made because of the overlap resulting from the limited resolution and the lack of full three-dimensional data. However, a rough estimate indicates that these extra peaks represent a magnetic moment of between 5 to 10% of the

TABLE VII. Superexchange paths involving the SO_4^{2} ion in $CuSO_4$. J_0, J_1, and J_2 represent exchange interactions between Cu at (0,0,0) and Cu′ as defined below [see, also, Fig. 8(b)]. N is the number of equivalent neighbors. The ideal angle is the value of the Cu-S-Cu angle in an ideal hexagonal lattice.

	Position Cu′	Superexchange path	Cu-S (Å)	S-Cu (Å)	Cu-S-Cu angle (deg)	Cu-Cu (Å)	Ideal angle (deg)	N	Coupling
J_0	$(\frac{1}{2},\frac{1}{2},0)$	Cu-O-(III)-S-O-(II)-Cu	3.17	3.14	100.2	4.84	90.0	4	F
		Cu-O(II)-S-O(I)-Cu	3.14	3.48	93.9				
	(1,0,0)	Cu-O(III)-S-O(I)-Cu	3.17	3.48	93.0	4.83	90.0	2	F
J_1	$(0,0,\frac{1}{2})$	Cu-O(II)-S-O(II)-Cu	3.14	3.14	64.5	3.35	70.5	2	AF
		Cu-O(III)-S-O(III)-Cu	3.17	3.17	63.7				
		Cu-O(I)-S-O(I)-Cu	3.48	3.48	57.6				
J_2	$(\frac{1}{2},\frac{1}{2},\frac{1}{2})$	Cu-O(III)-S-O(II)-Cu	3.17	3.14	137.7	5.89	131.8	4	AF
		Cu-O(II)-S-O(I)-Cu	3.14	3.48	125.6				
	(1,0,$\frac{1}{2}$)	Cu-O(III)-S-O(I)-Cu	3.17	3.48	124.1	5.88	131.8	4	AF

moment at the Cu^{2+} positions, i.e., around 0.05–0.1μ_B. It is noteworthy that the peaks are all about 1 Å from the nearest oxygen positions.

Although the crystal structure of $CuSO_4$ is too complex and the experimental data too few to permit a meaningful correlation of the extra regions of covalent spin density with specific superexchange interactions, the results indicate directly that a covalent group such as the SO_4^{2-} ion can act effectively as an intermediary in coupling the moments of ions separated by relatively large distances. This is also reflected in the fact that the Néel point of $CuSO_4$ is about 36°K while that of $CuCl_2\cdot 2H_2O$ is only 4.3°K. In both compounds there are well separated c-axis chains of octahedrally coordinated Cu ions; in $CuCl_2\cdot 2H_2O$, however, the interaction between the chains is calculated to be about an order of magnitude less than that within the chains,[33,34] and deviations in the observed form factors[23] are considerably less than in the case of $CuSO_4$.

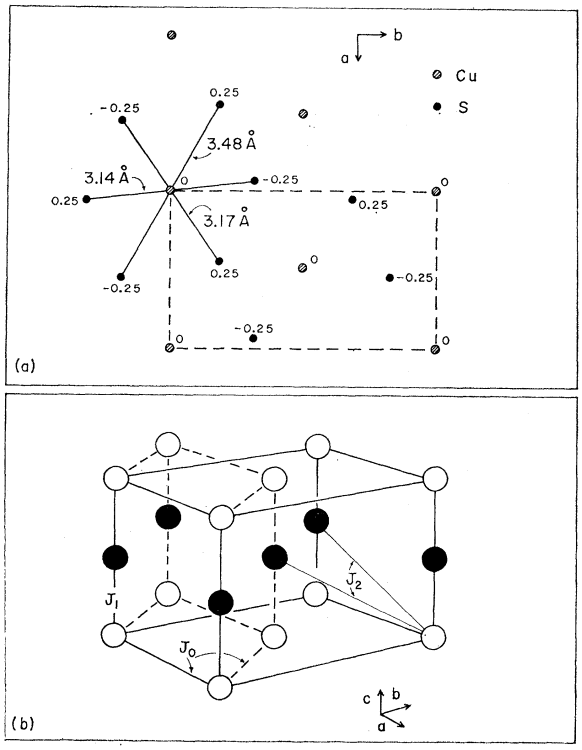

FIG. 8. (a) Projection of crystal structure on (001) showing the approximately hexagonal packing of Cu ions and SO_4 groups. Oxygens are omitted. Small numerals represent the z coordinates. (b) Superexchange paths between Cu ions in the ideal hexagonal approximation. The broken lines show the hexagonal pseudocell.

Table VII lists the possible superexchange paths via the sulfate group with appropriate distances and angles. If the sulfate ion is regarded as a single entity, the structure can be more easily visualized as a roughly hexagonal close-packed lattice of such ions with the Cu ions in octahedral sites [Fig. 8(a)]. This crude model is qualitatively useful in considering interactions between the Cu^{2+} ions, for in the ideal hexagonal case one need consider only three interactions: J_0 between pairs within an (001) plane, and J_1, and J_2 between nearest and next-nearest neighbors, respectively, in adjacent (001) planes [Fig. 8(b)]. The simple coupling-scheme envisaged by Uryu,[17] then corresponds to ferromagnetic J_0 and antiferromagnetic J_1; however, from Table VII it hardly seems justifiable to neglect J_2.

We may conclude then that the present experimental study has established that antiferromagnetic ordering in $CuSO_4$ is associated with the presence of substantial regions of unpaired electron density not localized on the magnetic Cu^{2+} ions, and which are directly suggestive of superexchange effects via the covalent sulfate groups.

ACKNOWLEDGMENTS

We wish to gratefully acknowledge the loan of a number of crystals of $CuSO_4$ from P. M. Gruzensky, of the NBS Boulder Laboratories, and many helpful discussions with R. E. Watson, M. Blume, R. Nathans, and G. Shirane. We also wish to acknowledge the help of W. C. Hamilton and Miss E. Wolfson in modifying the crystallographic least-squares program.

[33] W. Marshall, J. Phys. Chem. Solids 7, 159 (1958).
[34] A. C. Hewson, D. Ter Haar, and M. E. Lines, Phys. Rev. 137, A1465 (1965).